Load Alleviation of Flexible Aircraft by Dynamic Control Allocation

John H. Hansen,* Molong Duan,† Ilya V. Kolmanovsky,‡ and Carlos E. S. Cesnik§
University of Michigan, Ann Arbor, Michigan 48109

As wing designs aim for higher aerodynamic efficiency, the underlying aircraft structure becomes more flexible, requiring additional features to alleviate the loads encountered from gusts and maneuvers. While alleviating loads, it is desirable to minimize the deviations from the original flight trajectory. In this work, a dynamic control allocation method that exploits redundant control effectors for maneuver and gust load alleviation is proposed for flexible aircraft. The control architecture decouples the two objectives of load alleviation and rigid-body trajectory tracking by exploiting the null space between the input and the rigid-body output. A reduced-dimensional null space input is established, which affects the flexible output (but not the rigid-body output) when passed through a null space filter to generate incremental control signals. This null space input is determined by model predictive control to maintain the flexible output of the aircraft within specified values, thereby achieving load alleviation. Numerical simulations are used to illustrate the operation of this load alleviation system on nonlinear models. It is shown that the proposed load alleviation system can successfully avoid the violation of load bounds in the presence of both gust disturbances and maneuvers with minimal effect on the trajectory tracking performance.

I. Introduction

AIRCRAFT designed for increased fuel efficiency increasingly rely on high-aspect-ratio wings and lightweight structural characteristics. However, these design features often result in increased structural flexibility. A key challenge arising from increased flexibility is structural yielding or failure when the aircraft is subjected to aggressive flight maneuvers or gusts. Methods to alleviate the maneuver and gust loads on aircraft have been developed that are referred to as maneuver load alleviation (MLA) and gust load alleviation (GLA). While load alleviation (LA) helps to preserve the aircraft structural integrity, another objective is to maintain the aircraft maneuvering performance and trajectory tracking. Adverse effects on the maneuvering performance may lead to poor handling qualities or even affect how well the aircraft can complete its mission.

Several methods for LA have been proposed using both hardware and software. Solutions that involve additional or dedicated hardware [1–3] are preferably included in the design phase of an aircraft life cycle, rather than the sustainment phase. Adding new hardware to existing aircraft requires structural redesign, additional manufacturing, and testing, which may come at a high cost. Therefore, software solutions exploiting the existing control effectors are also appealing.

Early MLA software systems symmetrically deflected the wing control surfaces (e.g., ailerons, flaps) based on aircraft normal acceleration to reduce structural loads [4]. An MLA efficiency study by Yang et al. [5] found that the efficient deflection is down for inboard control surfaces and up for outboard ones. This moves the wing load toward the fuselage of a conventional transport aircraft, reducing the bending moment at the root of the wing. Similar to MLA, GLA also relies on the control surfaces to reduce the load, but it may not lead to symmetric deflections. Also, GLA typically requires a faster response to unanticipated dynamic loads [6]. To enable more effective use of multiple control surfaces for LA, several advanced control approaches have been proposed [7–13]. These approaches either allow or ignore the effects of the LA system on the flight trajectory tracking. Therefore, an alternate approach for handling multiple objectives is desirable.

One enabling characteristic for LA is that the aircraft often has more control inputs than the number of rigid-body degrees of freedom, which are controlled to follow specific trajectories. This redundancy is referred to as overactuation, and it allows the control inputs to be optimally arranged to handle multiple objectives using control allocation techniques. The control allocation structure is usually comprised of two stages: The first stage is a high-level controller that guarantees the desirable output (e.g., flight trajectory tracking), whereas the second stage is a detailed allocator satisfying a secondary objective (e.g., LA) [14]. Control allocation literature categorizes the dynamic system's input redundancy as either strong or weak. A system has strong input redundancy when it is possible to inject an arbitrary signal in certain input directions without affecting the state response of the plant. A system has weak input redundancy when this arbitrary signal does not affect the steady-state output of the system [15]. Strong input redundancy is commonly seen when the number of control inputs exceeds the number of internal states of the system dynamics. In contrast, for weak input redundancy, the number of control inputs typically exceeds the number of controlled outputs.

Control allocation methods that exploit strong input redundancy have been previously proposed for the control of rigid aircraft. The secondary objective for such a scenario is often something other than structural LA (e.g., control effector saturation avoidance [16–19], fault tolerance for control effectiveness uncertainty [20,21], or even thermal load management [22]). However, several examples with an objective of structural LA for rigid aircraft are more relative to this work [23–25]. These control allocation methods assume a static relationship between the structural load and the control inputs. Therefore, they may not be effective in regulating dynamic loads with pronounced transient characteristics as in flexible and very flexible aircraft. For this purpose, control allocation methods that exploit weak input redundancy are needed.

Gaulocher et al. [26] proposed a method based on model predictive control (MPC) to solve the dynamic optimal control allocation problem offline for a prescribed maneuver. A new control allocation law was then synthesized using a frequency-domain identification method based on the results from the offline optimization. Pereira

et al. [27] proposed two control system designs using MPC for MLA. One design directly provided a control allocation signal based on state feedback and load constraints. A second design used MPC to manipulate actuators pre-assigned to LA and the reference commands before they were sent to a linear quadratic regulator controller in the inner loop. Both designs used cost functions to minimize control use along with tracking error and successfully enforced bending constraints. Wang et al. [28,29] proposed a control system design using incremental nonlinear dynamic inversion with quadratic programming control allocation and virtual shape functions for MLA and GLA of flexible aircraft. Test results showed that the designed control allocator (CA) provided an optimal solution while satisfying actuator position constraints, rate constraints, and relative position constraints. Hashemi and Nguyen [30] proposed a two-part control system for longitudinal command tracking that includes an adaptive control component to reduce maneuver loads. One controller handles the trajectory tracking while a secondary adaptive controller focuses on reducing the resultant maneuver loads, but unfortunately disrupts the trajectory tracking performance.

As shown by this last example, the above methods still include some sort of tradeoff between trajectory tracking performance and LA. This occurs because these methods do not explicitly exploit the structure of input redundancy to decouple the two objectives of LA and trajectory tracking. Cocetti et al. [31] proposed a dynamic input allocator that directly exploits the input redundancy of a system for the purpose of input optimization. In this architecture, the dynamic input allocator works in the same control loop as a nominal controller to find the most suitable input trajectory based on certain performance criteria (e.g., energy minimization or saturation avoidance), while maintaining the same system output.

Duan and Okwudire [32,33] developed an energy-optimal dynamic control allocation method for multi-input, multi-output, linear time-invariant (LTI) overactuated systems using an optimal subspace that exploits the weak input redundancy of the system. This optimal subspace reflects an internal relationship within the null space between reference commands and desired output within which optimal control inputs can be found. Duan and Okwudire used matrix fraction description and spectral factorization to define a causal and stable proxy signal that measures the deviation from the optimal subspace. Then, optimal control trajectories were found by minimizing the proxy signal using $\mathcal{H}_\infty$ synthesis. This resulted in significant improvements in energy efficiency without affecting system outputs. The proposed method was designed to improve performance during prescribed mechanical processes (e.g., in additive manufacturing), which led to solutions based on the entire duration of the process. However, this method was limited by linear assumptions and lack of robustness consideration. Therefore, methods to shape the solutions considering the transients and nonlinear dynamics, as in the application of aircraft maneuvers and gust encounters, are needed.

Early GLA approaches used gust angle measurements at the nose of the aircraft to tailor the aircraft's gust response [34]. More recently, light detection and ranging (LIDAR) devices have been proposed to measure atmospheric disturbances ahead of an aircraft in order to provide a forecast for the control system [35–38].

In this work, a dynamic control allocation method for unified LA is proposed for weakly input redundant flexible aircraft. It is based upon the proxy-based optimal dynamic control allocation method developed by Duan and Okwudire [32,33]. This work is distinct from the architecture proposed in [31] in that it is designed for a system with two distinct output types, where the CA exploits the null space of one output type (in the primary control loop) in order to control the other output type using an auxiliary control loop. In this way, the control architecture decouples the two objectives of LA and rigid-body trajectory tracking. It is assumed that a desired maneuver trajectory and the gust profile for the near future are known a priori (e.g., through measurements with a LIDAR for the gust). This assumption facilitates the development of a unified LA solution for both maneuver and gust loads.

In the authors' previous conference papers [39,40], the proposed LA system was developed based on linearized models and demonstrated using linear simulations. The concept was first implemented with a full-knowledge preview of an aircraft maneuver [39]. A receding horizon approach was then developed to increase robustness and accommodate gust disturbances and maneuvers with limited preview [40]. The receding horizon control allocation approach is used to inform the MPC-based CA presented in this paper. The CA function operates as an add-on scheme to a nominal controller that facilitates the implementation of the proposed approach on the actual nonlinear system. The efficacy of the proposed method is demonstrated through numerical simulations on the Generic Transport Aircraft (GTA) nonlinear model, modified from [41].

II. Load Alleviation System Description

The block diagram of the proposed system is shown in Fig. 1. We assume that the flexible aircraft G is controlled to track a specified rigid-body output trajectory $r(t) \in \mathbb{R}^{n_r}$, in the presence of gust disturbance, $g(t) \in \mathbb{R}^3$, from longitudinal, vertical, and lateral directions, $0 \leq t \leq T_p$, where T_p is the preview horizon. The values of the inputs for maneuvers and gust disturbances are assumed to be known a priori over T_p, which is shorter than the total maneuver time T_{man}. The tracking is realized through a nominal controller C, which uses only the rigid-body output y_r for feedback and generates an n_u-dimensional control input u_0. The reference commands provided to the nominal controller and gust disturbance, along with the y_r feedback signal, produce a rigid output trajectory, $y_r(t) \in \mathbb{R}^{n_r}$, $0 \leq t \leq T_p$ and a flexible output trajectory, $y_f(t) \in \mathbb{R}^{n_f}$, $0 \leq t \leq T_p$.

Note that the model of the flexible aircraft G has a large state dimension to represent aeroelastic behavior, and the system has weak input redundancy. This provides an opportunity to control the flexible outputs of the system y_f without affecting tracking performance (i.e., the relationship between r, g, and the resulting y_r).

The implementation of the control allocation framework is based on two steps: i) the offline generation of a null space filter, which is designed so that the control input increment Δu produced as an output of this null space filter does not affect the rigid-body output y_r, and ii) online generation of a null space variable trajectory v, which is an input to the null space filter and enforces the bounds on y_f using a preview of the trajectory of the flexible output with the nominal controller. As Fig. 1 illustrates, these two functions are realized through two highlighted blocks N and L. The dotted lines in the figure represent signals that include data forecasted for the preview horizon. This CA incrementally adds Δu to the u_0 signal from the nominal controller, which simplifies the design and tuning process.
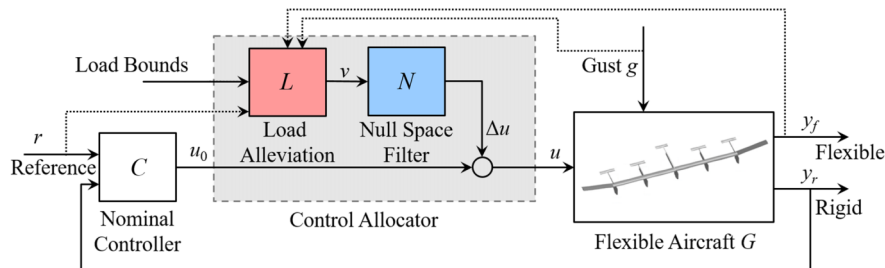

Fig. 1 Block diagram of load alleviation through control allocation architecture, including gust disturbances.

When considering this LA system, as shown in Fig. 1, one can see that there are two different ways to relate the signal from the CA to the rest of the system, and thus there are two options for maintaining continuity between implementation intervals. One method is to consider the null space variable $v(t)$ as the external input signal; this approach was used in [40]. The other method is to consider the $\Delta u(t)$ signal as the external input. The former option integrates the dynamics of the null space filter as a part of the closed loop system, and thus requires that the internal state of the null space filter be maintained to ensure continuity of the system output when advancing from one implementation interval to the next in the receding horizon implementation. The latter option maintains the $\Delta u(t)$ trajectory between implementation intervals, which is determined by passing the $v(t)$ signal through the null space filter (i.e., running a linear simulation for $\Delta u = N(s)v$). This shift from using $v(t)$ to $\Delta u(t)$ as one of the primary inputs to the system in controlling the flexible output, $y_f(t)$, has the added benefit that the initial condition for new implementation intervals has a physical meaning and corresponds to the extra utilization of the control effectors resulting from the $\Delta u(t)$ signal. To accommodate this change, the following modifications are necessary.

Assuming a linear model for the aircraft, we consider the transfer function representation for its input-output behavior in the form

$$
\begin{bmatrix} y_f(s) \\ y_r(s) \end{bmatrix} = \underbrace{\begin{bmatrix} G_{\text{fu}}(s) & G_{\text{fg}}(s) \\ G_{\text{ru}}(s) & G_{\text{rg}}(s) \end{bmatrix}}_{G(s)} \begin{bmatrix} u(s) \\ g(s) \end{bmatrix} \tag{1}
$$

where $y_r(s)$ and $y_f(s)$ are the rigid-body and flexible outputs of the system, respectively, resulting from the input $u(s)$ and gust $g(s)$. Let $y_f(t)$, $t \geq 0$, denote the time-domain solution of the flexible output of the aircraft model, which can be decomposed into a summation of the contributions from initial conditions and various inputs, i.e.,

$$
y_f(t) = y_{f_0}(t, x_{\text{CL}}(0)) + y_{\text{fr}}(t, r(t)) + y_{\text{fg}}(t, g(t)) \\ + y_{f\Delta u}(t, \Delta u(t)) \tag{2}
$$

where $y_{\text{fr}}(t)$ is the component of the flexible output from the reference signal, and $y_{\text{fg}}(t)$ and $y_{f\Delta u}(t)$ are similar components from the gust and incremental control input signals, respectively. The $y_{f_0}(t, x_{\text{CL}}(0))$ component of the flexible output corresponds to the initial condition of the closed-loop internal state $x_{\text{CL}}(0)$, which includes states from the aircraft model and the nominal controller. Based on Eq. (2) and the load bounds yields the following constraints:

$$
y_f^- \leq y_f(t) \leq y_f^+ \Leftrightarrow
$$
$$
y_{f\Delta u}(t, \Delta u(t)) \geq y_f^- - y_{f_0}(t, x_{\text{CL}}(0)) - y_{\text{fr}}(t, r(t)) - y_{\text{fg}}(t, g(t)),
$$
$$
y_{f\Delta u}(t, \Delta u(t)) \leq y_f^+ - y_{f_0}(t, x_{\text{CL}}(0)) - y_{\text{fr}}(t, r(t)) - y_{\text{fg}}(t, g(t)) \tag{3}
$$

The trajectory for $\Delta u(t)$ is indirectly calculated over the preview horizon, by determining a minimum 2-norm squared signal $v(t)$, $0 \leq t \leq T_p$, and then passing it through the null space filter (with zero initial conditions) to obtain $\Delta u(t)$, i.e., $\Delta u = N(s)v$, subject to the constraints in Eq. (3). Computationally, after time discretization with step T_s, this reduces to a quadratic programming (QP) problem and only the first value in the solution sequence is applied to the system. Then the process is repeated for the next time instant. In this way, the entire maneuver over the time interval $[0, T_{\text{man}}]$ is iteratively constructed.

A computationally efficient solution is obtained when the objective function to be minimized is chosen as the square of the 2-norm of the difference $\delta\Delta u_k(t)$ relative to an assumed incremental control trajectory $\Delta u_{a,k}(t)$, i.e.,

$$
\Delta u_k(t) = \Delta u_{a,k}(t) + \delta\Delta u_k(t) \\ = \Delta u_{a,k}(t) + Nv_k(t) \tag{4}
$$

for $kT_s \leq t \leq kT_s + T_p$, where $k = 0, 1, 2, \ldots$ The nominal trajectory of $\Delta u_{a,k}(t)$ for $k = 0$ is zero and for $k \geq 1$ is informed by the trajectory of $\Delta u_{k-1}(t)$ as

$$
\Delta u_{a,k}(t) = \begin{cases} \Delta u_{k-1}(t + T_s), & 0 \leq t \leq T_p - T_s, \\ \Delta \tilde{u}_{a,k}(t), & T_p - T_s \leq t \leq T_p \end{cases} \tag{5}
$$

where $\Delta \tilde{u}_{a,k}(t)$ is a linear function of time with boundary values $\Delta u_{k-1}(T_p)$ and zero.

Inserting Eq. (4) into Eq. (3) shows how $v_k(t)$ is used to indirectly alter $\Delta u_{a,k}(t)$ based on the constraint violations arising from the $\Delta u_{a,k}(t)$ trajectory. Specifically, the load constraints can now be expressed in a form which is convenient for use in a QP problem, i.e.,

$$
\underbrace{G_{\text{fu}}N}_{H_{\text{fv}}} v(t) \geq y_f^- - y_{f_0}(t, x_{\text{CL}}(0)) - y_{\text{fr}}(t, r(t)) - y_{\text{fg}}(t, g(t))
$$
$$
- y_{f\Delta u_a}(t, \Delta u_a(t)),
$$
$$
\underbrace{G_{\text{fu}}N}_{H_{\text{fv}}} v(t) \leq y_f^+ - y_{f_0}(t, x_{\text{CL}}(0)) - y_{\text{fr}}(t, r(t)) - y_{\text{fg}}(t, g(t))
$$
$$
- y_{f\Delta u_a}(t, \Delta u_a(t)) \tag{6}
$$

When using a discrete-time implementation, filtering v_k with $H_{\text{fv}}(s)$ is represented by the multiplication of Toeplitz matrix $\mathbb{H}_{\text{fv}}$ and $\mathbb{V}_k$ (sampled $v(t)$ arranged in a single-column vector), as detailed in [39]. Therefore, this leads to the following QP problem:

$$
\begin{aligned} \min_{\mathbb{V}_k} \quad & \mathbb{V}_k^{\text{T}}\mathbb{V}_k, \\ \text{s.t.} \quad & \mathbb{H}_{\text{fv}}\mathbb{V}_k \leq y_f^+ - \mathbb{Y}_{f_0,k} - \mathbb{Y}_{\text{fr},k} - \mathbb{Y}_{\text{fg},k} - \mathbb{Y}_{f\text{D}u_{a,k}}, \\ & -\mathbb{H}_{\text{fv}}\mathbb{V}_k \leq -y_f^- + \mathbb{Y}_{f_0,k} + \mathbb{Y}_{\text{fr},k} + \mathbb{Y}_{\text{fg},k} + \mathbb{Y}_{f\text{D}u_{a,k}} \end{aligned} \tag{7}
$$

The constraints of this QP problem shape the $v(t)$ signal that will control the flexible output. The right-hand side of the constraints is informed by a comparison of the predicted trajectory of $y_f(t)$ to the flexible limits of the structure. The left-hand side of the constraints is informed by the dynamics of the combined system of the null space filter and aircraft model.

III. Load Alleviation System Adaptation for Use with Nonlinear Systems

The next step to prepare the LA system for use with more realistic aircraft representations is to consider its implementation on a nonlinear system. For maneuvers and gust disturbance encounters beginning at a given equilibrium condition, a linearized model of the aircraft at that condition is used to generate a null space filter. That combination of the linearized model, of the corresponding null space filter, and of the nominal controller are used to allocate the controls with the ultimate objective of alleviating the critical loads of the nonlinear aircraft. The University of Michigan's Nonlinear Aeroelastic Simulation Toolbox (UM/NAST), which uses a strain-based formulation to model elastic dynamics of aerospace structures in free flight [42], is used to represent the nonlinear dynamics of the system. This software program includes various modules used to determine input settings for stable flight conditions, analyze structural modes, or to create linearized versions of the nonlinear models. UM/NAST also has modules to run static or dynamic nonlinear simulations and can also be coupled with controllers defined using C++, Python, or MATLAB [43,44].

A. Implementing Load Alleviation in Nonlinear Simulations

To use MPC when applying the LA system to a nonlinear model, the notional preview simulation and the quadratic programming optimization portions of the system are compiled into a separate CA function that is used by the nominal controller. The nominal controller and CA function are MATLAB scripts that can connect

with the Python interface of UM/NAST. This CA function requires the current value of the full state of the nonlinear aircraft model, the current state value of any integrators used in the nominal controller, the time discretization, the value of prediction horizon, T_p, and a priori knowledge of the reference command trajectory and gust disturbance over the prediction horizon. The CA function also uses a library of pre-calculated systems and variables for use by the optimization. This library includes an LTI model for the flexible aircraft and its state, linearized about the flight condition at the beginning of the simulation, and the corresponding model for the null space filter based on that aircraft model. The library also includes a representation of the closed-loop dynamics of the aircraft coupled with the nominal controller which gives the flexible output, $y_f(t)$, for a given reference command trajectory input, $r(t)$ and gust disturbance, $g(t)$. The library also includes matrices used to represent the aircraft model coupled with the null space filter in Toeplitz form, H_{fv}, for use in the quadratic programming problem. The CA function maintains its own reckoning of the current $\Delta u(t)$ trajectory, in order to ensure continuity between time steps. The controller state is coupled with the current aircraft state to define the closed-loop state initial condition. The library also contains the trim values of the full state of the aircraft and matrices used to represent the aircraft model coupled with the null space filter in Toeplitz form, for use in the quadratic programming problem.

The CA function begins with an assumed $\Delta u_a(t)$ trajectory over the prediction horizon T_p, which is how the continuity of this signal is maintained between time steps. When initialized, this assumed trajectory is just zeros, but is afterward replaced by the optimal solution from the QP solver. The previews of $r(t)$ and $g(t)$ are concatenated and used as an input in a notional linear simulation of the closed-loop system of the aircraft coupled with the nominal controller to predict the flexible output $y_f(t)$ for the preview horizon T_p. The $\Delta u_a(t)$ trajectory is also used as an input for the aircraft model to predict the corresponding component of $y_f(t)$ over the prediction horizon of length T_p. These components are added together to find the combined prediction of $y_f(t)$ resulting from $r(t)$, $g(t)$, and the $\Delta u_a(t)$ trajectory. This prediction comprises the right-hand side of the constraints in Eq. (7).

The CA function then checks to see if the predicted $y_f(t)$ exceeds the user-specified constraint on the flexible output. If the constraint is violated at any time within the prediction horizon T_p, then the LA system is engaged, and the QP solver is used to determine an optimal $v(t)$ trajectory that will keep $y_f(t)$ within the imposed constraints based on the solution of Eq. (7) (assuming a feasible solution exists). The optimal $v(t)$ trajectory is used as an input for the null space filter to obtain a corrective $\delta\Delta u(t)$ trajectory, which is combined with the $\Delta u_a(t)$ trajectory to determine the final $\Delta u(t)$ trajectory (i.e., $\Delta u(t) = \Delta u_a(t) + \delta\Delta u(t)$). On the other hand, if the predicted $y_f(t)$ does not exceed the user-specified constraint, then the $\Delta u_a(t)$ trajectory is used as the final $\Delta u(t)$ trajectory. As with standard MPC, only the first time step of the optimal $\Delta u(t)$ trajectory is returned to the nominal controller and is added to the $u_0(t)$ value determined by the nominal control law (as shown in Fig. 1) to alleviate the loads. In subsequent uses of the CA function, the remainder of the final $\Delta u(t)$ trajectory is retained in memory to be used as the $\Delta u_a(t)$ trajectory for the next iteration of the CA function.

B. Disengagement of the Load Alleviation System

This LA system is designed to introduce an additional input signal to alleviate loads when needed, and disengage by removing the signal when it is not needed. During implementation, only the first time step of the $\Delta u(t)$ trajectory is used in the iteration in which it was developed. The remaining time steps of the trajectory are retained in memory to provide a starting point for subsequent iterations of the CA function. However, one additional time step of values needs to be appended to the retained trajectory in order to run the necessary nominal prediction simulations used by the MPC. The value of this last time step of the prediction can have a significant effect on the overall performance of the system, especially because any deviation from this value is penalized during the QP process. Because the

overall objective of the LA system is to introduce a $\Delta u(t)$ only when necessary, the value for this last time step should represent an overall reduction toward zero, for each input channel.

The values of the $\Delta u(t)$ signal are directly connected to the activation of the aircraft control effectors, because the signal is downstream from the null space filter. This means that the decay of this signal may adversely affect the rigid-body output of the system. Therefore, care should be taken to reduce the trajectory gradually in order to minimize the effect on the rigid-body output of the aircraft. If a previous $\Delta u(t)$ trajectory is retained, the value of the next-to-last time step may be multiplied by a scalar value $k_{\Delta u}$ to prescribe the last time step of the preview horizon, i.e.,

$$\Delta u_{a,k}(t) = \begin{cases} \Delta u_{k-1}(t+1), & 0 \le t \le T_p - 1, \\ k_{\Delta u}\Delta u_{k-1}(t), & t = T_p \end{cases} \qquad (8)$$

If no further optimization of the $\Delta u(t)$ trajectory is needed in subsequent iterations of the CA function, this iterative scaling down of the final time step results in an exponential decay of the $\Delta u(t)$ trajectory and a disengagement of the LA system. The magnitude of the scalar value affects the rate of exponential decay. If the magnitude is too small, the signal will be removed too rapidly, which may result in large oscillations of $y_r(t)$. If the magnitude is too large, the LA system will remain engaged much longer than necessary or may result in too much compensation being used. Therefore, a magnitude within the range of 0.8–0.98 may provide the most desirable disengagement of the LA system, while minimizing adverse effects to the rigid output.

IV. Numerical Demonstration Using a Generic Transport Aircraft Model

The methods for LA discussed and derived in this work are numerically demonstrated using the GTA model, modified from [41]. This nonlinear model is firstly defined for use with UM/NAST, and a linearized model is generated to define its LA system.

A. Generic Transport Aircraft Model and Nominal Control

As illustrated in Fig. 2, the GTA is equipped with two elevators (ELV_L, ELV_R), two ailerons (AIL_L, AIL_R), one rudder (RDR), two flaps (FLP_L, FLP_R), and two thrusters (T_L, T_R). In total, this comprises nine control inputs to the system, i.e., $n_u = 9$. Accordingly, the control input u is defined as

$$u = [ELV_R \ \ ELV_L \ \ RDR \ \ AIL_R \ \ AIL_L \ \ FLP_R \ \ FLP_L \ \ T_R \ \ T_L]^{\mathrm{T}}$$

$$(9)$$

Note that the flaps in this model are defined identically to the ailerons, just located closer to the fuselage. This means that they are not restricted to only deflect trailing-edge down and are not rate limited to move more slowly than ailerons. The vector of rigid-body outputs to be controlled consists of the roll, pitch, and yaw angular rates, i.e.,
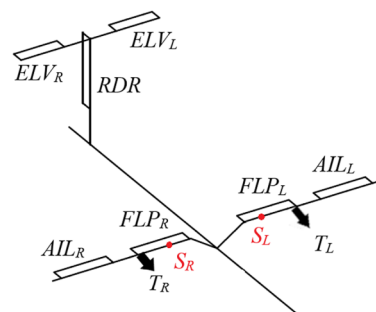

Fig. 2 Control inputs and critical stations on the Generic Transport Aircraft.

$$y_r = [\, p \quad q \quad r \,]^T \tag{10}$$

which means that $n_r = 3$. With $n_u > n_r$, the GTA also has the characteristics to support weak input redundancy.

The fuselage of the GTA is 22 m long with a diameter of 2.2 m. The wingspan is 19 m, with a constant chord of 2.2 m, giving it an aspect ratio of 8.6. The critical stations to evaluate the flexible outputs are defined as S_L and S_R, which are 2.25 m away from the center of the fuselage (see Fig. 2). The vector of flexible outputs, y_f, is composed of the out-of-plane bending curvatures at the critical stations, i.e.,

$$y_f = [\, \kappa_{L1} \quad \kappa_{R1} \,]^T \tag{11}$$

The stiffness of the GTA wings was numerically reduced from the design originally proposed in [41] so that the resulting model is more flexible and demonstrates geometric nonlinearities. A linearized model is generated at a trimmed condition of straight, level, unaccelerated flight using UM/NAST. The trim airspeed is 160 m/s, with an angle of attack of 1.8° at an altitude of 20,000 ft (6096 m). At this condition, the wings already have a deformed shape, with the highest out-of-plane bending curvature occurring at locations S_L and S_R. The curvatures for wing locations closer to the fuselage or the wing box inside the fuselage have a much smaller static deflection. The curvature for wing locations further outboard steadily decreases, approaching zero near the wingtip. At this condition, the baseline vertical wingtip deflection is 20.0% of half the aircraft wingspan. The first out-of-plane bending frequency is 1.37 Hz. As for rigid-body flight dynamics, the short-period frequency is 0.86 Hz, as determined by numerical simulation, using a high-magnitude elevator deflection of $-13°$ for 0.3 s. In terms of the flexible output of the system, the out-of-plane wing bending curvature has a static value of -0.118 1/m at this flight condition. This bending curvature is the main objective for the LA system to control within given structural bounds.

The nominal controller for the GTA stabilizes the rigid-body output of roll, pitch, and yaw rates using decoupled proportional-integral (PI) controllers for each axis. These PI controllers generate τ_p, τ_q, and τ_r, which inform required control actions for roll, pitch, and yaw axes, respectively, i.e.,

$$
\begin{aligned}
\tau_p &= \left(K_{pp} + \frac{K_{pi}}{s} \right)(r_p - y_p), \\[4pt]
\tau_q &= -\left(K_{qp} + \frac{K_{qi}}{s} \right)(r_q - y_q), \\[4pt]
\tau_r &= \left(K_{rp} + \frac{K_{ri}}{s} \right)(r_r - y_r)
\end{aligned}
\tag{12}
$$

These signals are directly fed to the control channels identified in Eq. (9), deflecting the ailerons asymmetrically [i.e., $AIL_R(t) = -\tau_p(t)$ and $AIL_L(t) = \tau_p(t)$], deflecting both elevators symmetrically [i.e., $ELV_L(t) = ELV_R(t) = \tau_q(t)$], and deflecting the rudder by $\tau_r(t)$. This represents a heuristic baseline control allocation structure. The input channels for the thrusters and flaps are not controlled by the nominal controller, and would be direct feedthrough from the operator. However, all input channels are available for the CA, through the $\Delta u(t)$ signal. All control surfaces are given a maximum deflection limit of $\pm 45°$. Note that this design only uses the feedback of the rigid-body angular rates, which satisfies the specification of separating the rigid and flexible outputs in Fig. 1. The gains of the PI controller are provided in Table 1.

The reference command signal $r(t)$ and gust disturbance signal $g(t)$ are contained in lookup tables in a database, which is accessed by the nominal controller. The sensor data and reference signal, according to the control law, generate a nominal control signal $u_0(t)$. The nominal controller must also use the CA function to obtain the $\Delta u(t)$ vector.

Table 1 Gains of GTA nominal controller

Gain	Value
K_{pp}	1.0 s
K_{pi}	10.0
K_{qp}	0.3 s
K_{qi}	3.0
K_{rp}	3.0 s
K_{ri}	7.0

B. Performance Metrics for Numerical Demonstration

The following performance metrics are defined in order to quantify the performance of the LA system through numerical simulations.

The first performance metric describes the amount of correction needed by the LA system in order to attenuate the flexible output within the user-defined bounds when performing the maneuver without the LA system. This metric is expressed as a percentage of the maximum flexible output displacement from the equilibrium value before the maneuver or gust disturbance, i.e.,

$$y_{f,\text{correction}} = \frac{y_f^- - \hat{y}_{f\,\text{min}}}{\hat{y}_{f\,\text{min}} - y_{f\text{eq}}} \tag{13}$$

where $\hat{y}_{f\,\text{min}}$ is the minimum observed flexible output from the maneuver without the LA system, and $y_{f\text{eq}}$ is the value of the flexible output at the equilibrium condition, before the maneuver is initiated or gust disturbance is encountered.

The next performance metric corresponds to the primary objective of LA. It describes the margin between the flexible output and the user-defined constraint during the maneuver or gust encounter. After running a numerical simulation with the LA system engaged, the minimum observed value of the flexible output will be compared to the user-defined constraint. This results in a flexible output integrity metric, expressed as a percentage of the maximum flexible output displacement from the equilibrium value:

$$y_{f,\text{integrity}} = \frac{y_f^- - y_{f\,\text{min}}}{\hat{y}_{f\,\text{min}} - y_{f\text{eq}}} \tag{14}$$

where $y_{f\,\text{min}}$ is the minimum observed flexible output during the maneuver or gust disturbance encounter with the LA system engaged. Any instance where the integrity metric has a value less than zero represents a constraint violation. The closer this value is to zero can be thought of as a measure of optimality, meaning that the LA system adjusted the control allocation enough to meet the constraints, but not to excess.

The final performance metric corresponds to the secondary objective of the proposed LA system: preserving rigid-body trajectory tracking performance. A distinguishing feature of the system under evaluation is the exploitation of the null space of the aircraft model, which enables changes to the flexible output without affecting the rigid-body output. However, this feature relies on the property of superposition for linear systems, which may not hold during the dynamic simulation of the nonlinear model. The rigid-body output data observed during the maneuver or gust disturbance encounter with the LA system engaged will be compared to the corresponding output data without the LA system engaged throughout the time history data log. Specifically, the difference between the rigid-body output values will be calculated starting from the first point in time where the mean $\Delta u(t)$ value of all input channels is greater than zero until the mean $\Delta u(t)$ value returns to zero, or the end of the data log. The mean of the absolute value of these differences will be calculated, resulting in a rigid-body output mean absolute error:

$$e_{y_r} = \frac{1}{n} \sum_{i=1}^{n} \| y_r(i) - \hat{y}_r(i) \| \tag{15}$$

where n is the number of time steps in the sample, and $\mathbf{y}_r(t)$ and $\hat{\mathbf{y}}_r(t)$ represent the rigid-body output data from the simulation with and without the LA system engaged, respectively. Ideally, this value should be as close to zero as possible.

C. Simulation Results

The system was simulated using the dynamic solver module of UM/NAST. The two test cases for this demonstration are described here.

1) *Descent:* To descend to a lower altitude, the reference trajectory consists of a pitch down 2 s after the simulation starts with a pulse of $-6°/s$ over 1 s. The nose-down pitch attitude is held for 4 s before leveling off in one additional second. This maneuver results in a descent of 80 m.

2) *Descent with discrete gust encounter:* While leveling off during the descent maneuver described above, the aircraft encounters a discrete upward gust with a $1-$cosine profile. The gust is encountered 8 s after the simulation starts, swelling to a peak gust amplitude of $U_0 = 10.8$ m/s and then decaying to zero over 1.03 s (i.e., $t_{gust} = 1.03$ s). The parameters for this gust are based on the airworthiness specifications for critical gust loads described in Title 14 of the CFR, section 25.341 [45].

Additional trajectories that did not include a pitch component were explored but did not sufficiently excite the bending curvature beyond the bound. The LA system was not engaged by such trajectories; therefore, those results are not shown.

The nonlinear model is built using UM/NAST, and the required input settings for level flight are determined and applied for a dynamic simulation with a time discretization of 0.01 s. The controller is written in a MATLAB script (ver. r2020a [46]), based on the PI control architecture described in Sec. IV.A. The controller script obtains the reference command signal from a lookup table. This controller script also calls the CA function, which utilizes MPC (with $T_p = 3$ s) to find the appropriate $\Delta\mathbf{u}(t)$ value for each time step. The CA function is configured to retain the $\Delta\mathbf{u}(t)$ solution each iteration to maintain continuity. The disengagement mechanism is an exponential decay of the $\Delta\mathbf{u}(t)$ signal at the end of the last solution from the QP solver, as described in Sec. III.B, with $k_{\Delta u} = 0.95$. For this demonstration, the null space filter is invariant and is generated based on the equilibrium point conditions and linearized model at the beginning of the simulation. The bound on the wing bending curvature is set to -0.235 m^{-1} for both test cases. This value represents a flexible output correction factor of $y_{f,\text{correction}} = 11.1\%$, according to Eq. (13).

The state results for test case 1), both with and without LA, are shown in Fig. 3. The rigid-body outputs of roll, pitch, and yaw rates are on the left. The aircraft load factor is on the bottom right, and the flexible outputs for each wing are on the upper right. The time histories of the elevator, aileron, and flap inputs are shown in Fig. 4. The solution had only an inconsequential effect on the nominal control signal for the rudder and thrusters; therefore, they are not displayed.

The plot for the bending curvature shows that the constraint is satisfied with a reasonable margin, which represents an attenuation of over 20% of the bending, compared to the results without LA. The bending curvature integrity metrics for the left and right wings are $\kappa_{L,\text{integrity}} = 12.9\%$ and $\kappa_{R,\text{integrity}} = 10.5\%$, respectively. There is some extraneous motion in the roll axis, which is interesting because the maneuver is purely longitudinal and the aircraft model is symmetric about the longitudinal axis. The research team attempted to force a symmetric response by the LA system by adding additional constraints to the QP solver for Eq. (7), but no feasible solution could be found. This suggests that asymmetric behavior is a result of the characteristics of the null space filter created from this linearized model of the aircraft. Indeed, a Fourier transform spectral analysis of the null space filter showed that the output channel for roll rate had a higher signal power than the other rigid-body output channels. This result shows that different null space filters can have different characteristics that may provide an improved performance for the LA system. Other methods of manipulating the objective model to generate a null space filter may produce a better filter than the one used for this study, but the one used for this study provided the best result of the several potential null space filters investigated. Overall, the results are very desirable, with mean absolute errors of $e_p = 0.060$ deg/s, $e_q = 0.040$ deg/s, and $e_r = 0.006$ deg/s, for the roll, pitch, and yaw rates, respectively.

The resultant $\Delta\mathbf{u}(t)$ can be approximated by noting the difference between the plots in Fig. 4. When the $\Delta\mathbf{u}(t)$ signal is active, the elevators deflect less, which would provide less pitch rate. Both ailerons deflect upward, though the left aileron has a larger deflection than the right, which may be the source of the roll-rate error observed in Fig. 3. A deflection in the same direction, such as this, would reduce the lift near the wingtips. Simultaneously, the flaps deflect
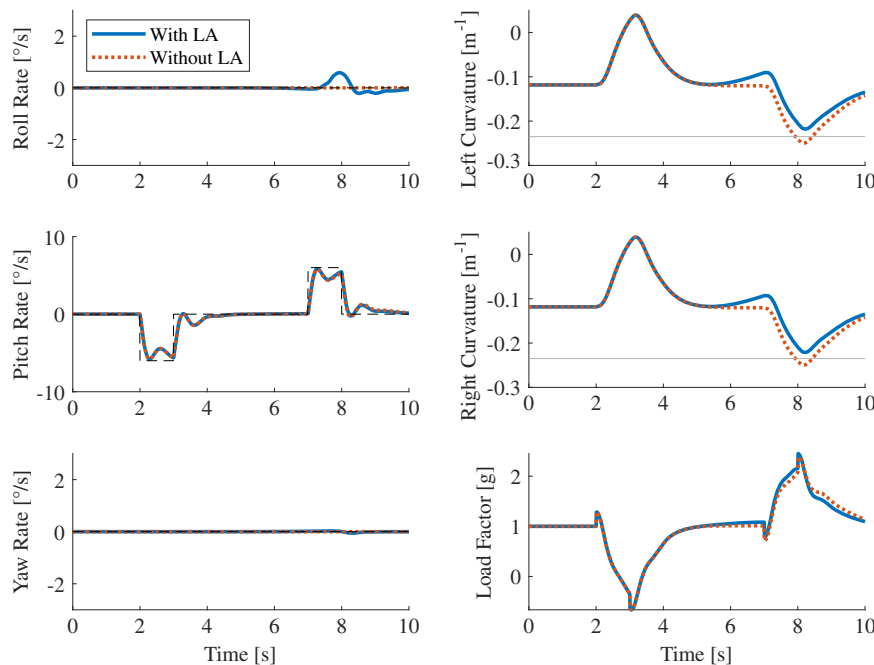

Fig. 3 Responses of rigid-body motion and wing root bending curvature for descent for an invariant null space filter applied to a nonlinear GTA model, with and without LA.
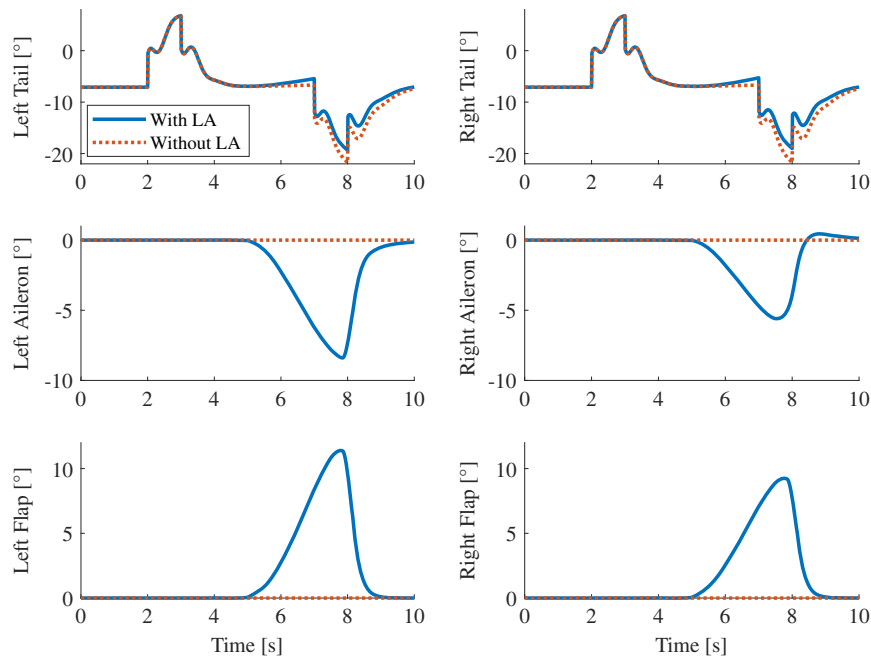
Fig. 4   Time histories of elevator, aileron, and flap inputs for descent for an invariant null space filter applied to a nonlinear GTA model, with and without LA.

downward, increasing the lift near the fuselage. This matches the conclusions found in the literature for centrally loaded aircraft [5]. One interesting result is the difference in load factor with the LA system active. The measured load factor comes from a simulated inertial navigation sensor placed at the center of the fuselage where it intersects the wing. The difference is small, but the value of the load factor is higher when the LA system is active, even while the wing bending curvature is being reduced. One way to understand this phenomenon is to first note that the pitch rate motion is approximately the same for both cases, meaning that the lifting force is staying the same. With that in mind, if the wings are not bent as much, then it means that the amount of force that would normally be absorbed by the wings flexing is instead being redirected to the fuselage, thus increasing the load factor measured there by the sensor.

The state results for test case 2, both with and without LA, are shown in Fig. 5. The time histories of the elevator, aileron, and flap inputs are shown in Fig. 6. The flexible state constraint was equal to the case without gust, which now represents a flexible output correction factor of $y_{f,\text{correction}} = 36.8\%$ of the bending, compared to the results without LA.

The plot for the bending curvature shows that the constraint is satisfied with plenty of margin. The resultant bending trajectory satisfied the constraints by an extra 21%, showing an overall attenuation of 58%, compared to the results without LA. The bending curvature integrity metrics for the left and right wings are $\kappa_{L,\text{integrity}} = 28.1\%$ and $\kappa_{R,\text{integrity}} = 21.3\%$, respectively. The LA objective is achieved, but the response is excessive, showing some areas for future improvement of the system. There is some extraneous motion
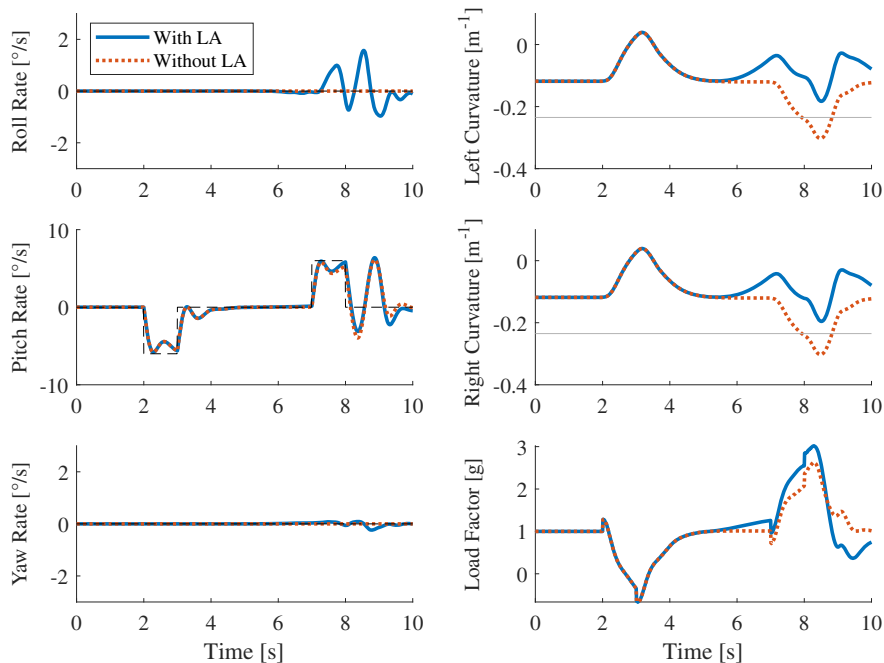

Fig. 5   Responses of rigid-body motion and wing root bending curvature for descent with discrete gust for an invariant null space filter applied to a nonlinear GTA model, with and without LA.
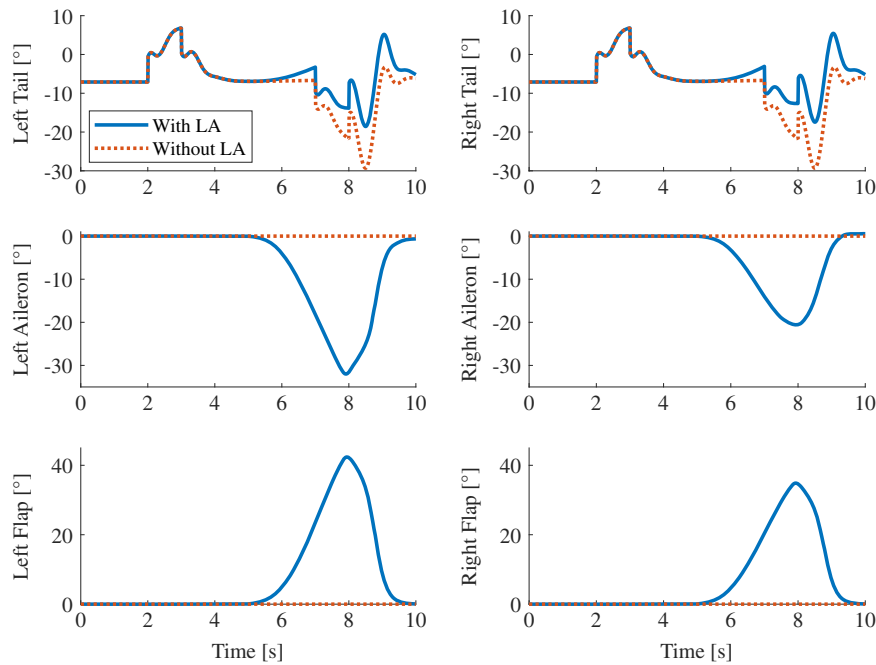
Fig. 6   Time histories of elevator, aileron, and flap inputs for descent with discrete gust for an invariant null space filter applied to a nonlinear GTA model, with and without LA.

in the roll and pitch axes, but it is still less than 0.2 deg/s. The mean absolute errors are $e_p = 0.156$ deg/s, $e_q = 0.153$ deg/s, and $e_r = 0.023$ deg/s, for the roll, pitch, and yaw rates, respectively.

The resultant $\Delta \boldsymbol{u}(t)$ can be approximated by noting the difference between the plots in Fig. 6. Compared to the observations for test case 1, the elevators deflect less, both ailerons deflect upward, and the flaps deflect downward, to reduce the out-of-plane wing bending. The relative increase in load factor is observed again.

V.   Conclusions

The LA method developed in this work exploits the null space between the reference input and the rigid-body output of a flexible aircraft to control the flexible output without affecting the tracking performance. By using the null space, the control architecture decouples the two objectives of LA and rigid-body trajectory tracking. For a given aircraft linearized model, a null space filter is generated so that its output signal can be sent to the aircraft control effectors without affecting the rigid-body output. A reduced-dimension null space variable is defined as the input to the null space filter and its trajectory is determined so that it can control the flexible output to remain within given constraints. Modifications were made to adapt the LA system for use with nonlinear aircraft models. These included modifying the previous approach with a model predictive control-based CA function that can run on top of a nominal controller and applies to nonlinear models and simulations. Numerical simulations were used to demonstrate the operation of this LA system using the GTA model. Numerical results showed the effect of using an MPC-based LA system on top of a nominal controller while running nonlinear dynamic simulations with the GTA model. Results using an invariant null space filter for a nonlinear GTA model overshot a 35% goal to attenuate the flexible output by an additional 20% while keeping mean absolute errors of the rigid-body outputs to less than 0.2 deg/s. These demonstrations showed that the LA system can successfully avoid the violation of flexible output constraints resulting from both gust disturbances and maneuvers with minimal effect on the trajectory tracking performance.

References

[1] Guo, S., Fu, Q., and Sensburg, O., "Optimal Design of a Passive Gust Alleviation Device for a Flying Wing Aircraft," *12th AIAA Aviation Technology, Integration, and Operations (ATIO) Conference*, AIAA Paper 2012-5625, 2012.
https://doi.org/10.2514/6.2012-5625

[2] Urnes, J., Nguyen, N., Ippolito, C., Totah, J., Trinh, K., and Ting, E., "A Mission Adaptive Variable Camber Flap Control System to Optimize High Lift and Cruise Lift to Drag Ratios of Future N + 3 Transport Aircraft," *51st AIAA Aerospace Sciences Meeting*, AIAA Paper 2013-0214, 2013.
https://doi.org/10.2514/6.2013-214

[3] Fonte, F., Toffol, F., and Ricci, S., "Design of a Wing Tip Device for Active Maneuver and Gust Load Alleviation," *2018 AIAA/ASCE/AHS/ASC Structures, Structural Dynamics, and Materials Conference*, AIAA Paper 2018-1442, 2018.
https://doi.org/10.2514/6.2018-1442

[4] White, R. J., "Improving the Airplane Efficiency by Use of Wing Maneuver Load Alleviation," *Journal of Aircraft*, Vol. 8, No. 10, 1971, pp. 769–775.
https://doi.org/10.2514/3.59169

[5] Yang, Y., Wu, Z., and Yang, C., "Control Surface Efficiency Analysis and Utilization of an Elastic Airplane for Maneuver Loads Alleviation," *54th AIAA/ASME/ASCE/AHS/ASC Structures, Structural Dynamics, and Materials Conference*, AIAA Paper 2013-1487.
https://doi.org/10.2514/6.2013-1487

[6] Xu, J., and Kroo, I., "Aircraft Design with Active Load Alleviation and Natural Laminar Flow," *Journal of Aircraft*, Vol. 51, No. 5, 2014, pp. 1532–1545.
https://doi.org/10.2514/1.C032402

[7] Dillsaver, M. J., Cesnik, C. E. S., and Kolmanovsky, I. V., "Gust Load Alleviation Control for Very Flexible Aircraft," *AIAA Atmospheric Flight Mechanics Conference*, AIAA Paper 2011-6368, 2011.
https://doi.org/10.2514/6.2011-6368

[8] Li, H., Zhao, Y., and Hu, H., "Adaptive Maneuver Load Alleviation via Recurrent Neural Networks," *Journal of Guidance, Control, and Dynamics*, Vol. 40, No. 7, 2017, pp. 1824–1831.
https://doi.org/10.2514/1.G002178

[9] Yagil, L., Raveh, D. E., and Idan, M., "Deformation Control of Highly Flexible Aircraft in Trimmed Flight and Gust Encounter," *Journal of Aircraft*, Vol. 55, No. 2, 2017, pp. 829–840.
https://doi.org/10.2514/1.C034353

[10] Kopf, M., Bullinger, E., Giesseler, H.-G., Adden, S., and Findeisen, R., "Model Predictive Control for Aircraft Load Alleviation: Opportunities and Challenges," *2018 Annual American Control Conference (ACC)*, 2018, pp. 2417–2424.
https://doi.org/10.23919/ACC.2018.8430956

[11] Haghighat, S., Liu, H. H. T., and Martins, J. R. R. A., "Model-Predictive Gust Load Alleviation Controller for a Highly Flexible Aircraft," *Journal of Guidance, Control, and Dynamics*, Vol. 35,

No. 6, 2012, pp. 1751–1766.
https://doi.org/10.2514/1.57013

[12] Wang, Y., Wynn, A., and Palacios, R., "Model-Predictive Control of Flexible Aircraft Using Nonlinear Reduced-Order Models," *AIAA Scitech 2016 Forum*, AIAA Paper 2016-0711, 2016.
https://doi.org/10.2514/6.2016-0711

[13] Zeng, J., Moulin, B., de Callafon, R., and Brenner, M. J., "Adaptive Feedforward Control for Gust Load Alleviation," *Journal of Guidance, Control, and Dynamics*, Vol. 33, No. 3, 2010, pp. 862–872.
https://doi.org/10.2514/1.46091

[14] Johansen, T. A., and Fossen, T. I., "Control Allocation—A Survey," *Automatica*, Vol. 49, No. 5, 2013, pp. 1087–1103.
https://doi.org/10.1016/j.automatica.2013.01.035

[15] Zaccarian, L., "Dynamic Allocation for Input Redundant Control Systems," *Automatica*, Vol. 45, No. 6, 2009, pp. 1431–1438.
https://doi.org/10.1016/j.automatica.2009.01.013

[16] Bodson, M., and Frost, S. A., "Load Balancing in Control Allocation," *Journal of Guidance, Control, and Dynamics*, Vol. 34, No. 2, 2011, pp. 380–387.
https://doi.org/10.2514/1.51952

[17] Härkegård, O., "Dynamic Control Allocation Using Constrained Quadratic Programming," *Journal of Guidance, Control, and Dynamics*, Vol. 27, No. 6, 2004, pp. 1028–1034.
https://doi.org/10.2514/1.11607

[18] Luo, Y., Serrani, A., Yurkovich, S., Oppenheimer, M. W., and Doman, D. B., "Model-Predictive Dynamic Control Allocation Scheme for Reentry Vehicles," *Journal of Guidance, Control, and Dynamics*, Vol. 30, No. 1, 2007, pp. 100–113.
https://doi.org/10.2514/1.25473

[19] Yildiz, Y., and Kolmanovsky, I., "Stability Properties and Cross-Coupling Performance of the Control Allocation Scheme CAPIO," *Journal of Guidance, Control, and Dynamics*, Vol. 34, No. 4, 2011, pp. 1190–1196.
https://doi.org/10.2514/1.50310

[20] Burken, J. J., Lu, P., Wu, Z., and Bahm, C., "Two Reconfigurable Flight-Control Design Methods: Robust Servomechanism and Control Allocation," *Journal of Guidance, Control, and Dynamics*, Vol. 24, No. 3, 2001, pp. 482–493.
https://doi.org/10.2514/2.4769

[21] Cui, L., and Yang, Y., "Disturbance Rejection and Robust Least-Squares Control Allocation in Flight Control System," *Journal of Guidance, Control, and Dynamics*, Vol. 34, No. 6, 2011, pp. 1632–1643.
https://doi.org/10.2514/1.52234

[22] Doman, D. B., Oppenheimer, M. W., and Rone, W., "Selective Self-Locking Actuator and Control Allocation Approach for Thermal Load Minimization," *Journal of Guidance, Control, and Dynamics*, Vol. 38, No. 6, 2015, pp. 1110–1118.
https://doi.org/10.2514/1.G000859

[23] Durham, W., Bordignon, K. A., and Beck, R., *Aircraft Control Allocation*, Wiley, Chichester, England, U.K., 2016, Chap. 5.

[24] Frost, S. A., Bodson, M., Burken, J. J., Jutte, C. V., Taylor, B. R., and Trinh, K. V., "Flight Control with Optimal Control Allocation Incorporating Structural Load Feedback," *Journal of Aerospace Information Systems*, Vol. 12, No. 12, 2015, pp. 825–834.
https://doi.org/10.2514/1.I010278

[25] Miller, C. J., and Goodrick, D., "Optimal Control Allocation with Load Sensor Feedback for Active Load Suppression, Experiment Development," *AIAA Guidance, Navigation, and Control Conference*, AIAA Paper 2017-1719, 2017.
https://doi.org/10.2514/6.2017-1719

[26] Gaulocher, S. L., Roos, C., and Cumer, C., "Aircraft Load Alleviation During Maneuvers Using Optimal Control Surface Combinations," *Journal of Guidance, Control, and Dynamics*, Vol. 30, No. 2, 2007, pp. 591–600.
https://doi.org/10.2514/1.25577

[27] Pereira, M. D. V., Kolmanovsky, I., Cesnik, C. E. S., and Vetrano, F., "Model Predictive Control Architectures for Maneuver Load Alleviation in Very Flexible Aircraft," *AIAA Scitech 2019 Forum*, AIAA Paper 2019-1591, 2019.
https://doi.org/10.2514/6.2019-1591

[28] Wang, X., Van Kampen, E., Chu, Q. P., and De Breuker, R., "Flexible Aircraft Gust Load Alleviation with Incremental Nonlinear Dynamic

Inversion," *Journal of Guidance, Control, and Dynamics*, Vol. 42, No. 7, 2019, pp. 1519–1536.
https://doi.org/10.2514/1.G003980

[29] Wang, X., Mkhoyan, T., Mkhoyan, I., and De Breuker, R., "Seamless Active Morphing Wing Simultaneous Gust and Maneuver Load Alleviation," *Journal of Guidance, Control, and Dynamics*, Vol. 44, No. 9, 2021, pp. 1649–1662.
https://doi.org/10.2514/1.G005870

[30] Hashemi, K. E., and Nguyen, N. T., "Adaptive Maneuver Load Alleviation for Flexible Wing Aircraft with Nonminimum Phase Zeros," *2018 AIAA Guidance, Navigation, and Control Conference*, AIAA Paper 2018-0619, 2018.
https://doi.org/10.2514/6.2018-0619

[31] Cocetti, M., Serrani, A., and Zaccarian, L., "Dynamic Input Allocation for Uncertain Linear Over-Actuated Systems," *2016 Annual American Control Conference (ACC)*, 2016, pp. 2906–2911.
https://doi.org/10.1109/ACC.2016.7525360

[32] Duan, M., and Okwudire, C., "Proxy-Based Optimal Dynamic Control Allocation for Multi-Input, Multi-Output Over-Actuated Systems," *Proceedings of the ASME 2017 Dynamic Systems and Control Conference*, ASME Paper 2017-5343, 2017.
https://doi.org/10.1115/DSCC2017-5343

[33] Duan, M., and Okwudire, C., "Proxy-Based Optimal Control Allocation for Dual-Input Over-Actuated Systems," *IEEE/ASME Transactions on Mechatronics*, Vol. 23, No. 2, 2018, pp. 895–905.
https://doi.org/10.1109/TMECH.2018.2796500

[34] Krag, B., Rohlf, D., and Wunnenberg, H., "OLGA. A Gust Alleviation System for Improvement of Passenger Comfort of General Aviation Aircraft," *Proceedings of the 12th Congress of the International Council of the Aeronautical Sciences (ICAS)*, 1980, pp. 219–231.

[35] Rabadan, G. J., Schmitt, N. P., Pistner, T., and Rehm, W., "Airborne Lidar for Automatic Feedforward Control of Turbulent In-Flight Phenomena," *Journal of Aircraft*, Vol. 47, No. 2, 2010, pp. 392–403.
https://doi.org/10.2514/1.44950

[36] Giesseler, H.-G., Kopf, M., Varutti, P., Faulwasser, T., and Findeisen, R., "Model Predictive Control for Gust Load Alleviation," *4th IFAC Nonlinear Model Predictive Control Conference*, Elsevier, 2012, pp. 27–32.
https://doi.org/10.3182/20120823-5-NL-3013.00049

[37] Vrancken, P. S., *Airborne Remote Detection of Turbulence with Forward-Pointing LIDAR*, Springer International Publishing, Cham, Switzerland, 2016, pp. 443–464.
https://doi.org/10.1007/978-3-319-23630-8_22

[38] Fezans, N., Joos, H.-D., and Deiler, C., "Gust Load Alleviation for a Long-Range Aircraft With and Without Anticipation," *CEAS Aeronautical Journal*, Vol. 10, No. 4, 2019, pp. 1033–1057.
https://doi.org/10.1007/s13272-019-00362-9

[39] Duan, M., Hansen, J. H., Kolmanovsky, I. V., and Cesnik, C. E. S., "Maneuver Load Alleviation of Flexible Aircraft Through Control Allocation: A Case Study Using X-HALE," *International Forum on Aeroelasticity and Structural Dynamics*, 2019, p. 109.

[40] Hansen, J. H., Duan, M., Kolmanovsky, I. V., and Cesnik, C. E. S., "Control Allocation for Maneuver and Gust Load Alleviation of Flexible Aircraft," *AIAA Scitech 2020 Forum*, AIAA Paper 2020-1186, 2020.
https://doi.org/10.2514/6.2020-1186

[41] Karpel, M., Shousterman, A., Maderuelo, C., and Climent, H., "Dynamic Aeroservoelastic Response with Nonlinear Structural Elements," *AIAA Journal*, Vol. 53, No. 11, 2015, pp. 3233–3239.
https://doi.org/10.2514/1.J053550

[42] Su, W., and Cesnik, C. E. S., "Dynamic Response of Highly Flexible Flying Wings," *AIAA Journal*, Vol. 49, No. 2, 2011, pp. 324–339.
https://doi.org/10.2514/1.J050496

[43] Pang, Z. Y., "Modeling, Simulation and Control of Very Flexible Unmanned Aerial Vehicle," Ph.D. Thesis, Univ. of Michigan, Ann Arbor, MI, 2018.

[44] Lupp, C., "Inclusion of Geometrically Nonlinear Aeroelastic Effects into Gradient-Based Aircraft Optimization," Ph.D. Thesis, Univ. of Michigan, Ann Arbor, MI, 2020.

[45] *Title 14 of the Code of Federal Regulations: Aeronautics and Space PART 25*, Federal Aviation Administration, Government Publishing Office, Washington, D.C., 1964.

[46] *MATLAB*, Ver. 9.8.0, The MathWorks, Inc., Natick, MA, 2010.